Combustion and Flame 161 (2014) 2469–2478

Contents lists available at ScienceDirect

Combustion and Flame

journal homepage: www.elsevier.com/locate/combustflame

Combustion of micron-sized aluminum particle, liquid water, and hydrogen peroxide mixtures

Dilip Srinivas Sundaram, Vigor Yang *

School of Aerospace Engineering, Georgia Institute of Technology, Atlanta, GA 30332, USA

ARTICLE INFO

Article history:
Received 13 January 2014
Received in revised form 2 March 2014
Accepted 3 March 2014
Available online 22 March 2014

Keywords:
Aluminum
Water
Hydrogen peroxide
Combustion
Model
Flame propagation

ABSTRACT

The combustion of aluminum particle, liquid water, and hydrogen peroxide (H_2O_2) mixtures is studied theoretically for a pressure range of 1–20 MPa and particle sizes between 3 and 70 μm. The oxidizer-to-fuel (O/F) weight ratio is varied in the range of 1.00–1.67, and four different H_2O_2 concentrations of 0%, 30%, 60%, and 90% are considered. A multi-zone flame model is developed to determine the burning behaviors and combustion-wave structures by solving the energy equation in each zone and enforcing the temperature and heat-flux continuities at the interfacial boundaries. The entrainment of particles is taken into account. Key parameters that dictate the burning properties of mixtures are found to be the thermal diffusivity, flame temperature, particle burning time, ignition temperature, and entrainment index of particles. When the pressure increases from 1 to 20 MPa, the flame thickness decreases by a factor of two. The ensuing enhancement of conductive heat flux to the unburned mixture thus increases the burning rate, which exhibits a pressure dependence of the form $r_b = ap^m$. The exponent, m, depends on reaction kinetics and convective motion of particles. Transition from diffusion to kinetically-controlled conditions causes the pressure exponent to increase from 0.35 at 70 μm to 1.04 at 3 μm. The addition of hydrogen peroxide has a positive effect on the burning properties. The burning rate is nearly doubled when the concentration of hydrogen peroxide increases from 0 to 90%. For the conditions encountered in this study, the following correlation for the burning rate is developed: $r_b[\mathrm{cm/s}] = 4.97(p[\mathrm{MPa}])^{0.37}(d_p[\mu\mathrm{m}])^{-0.85}(\mathrm{O/F})^{-0.54}\exp(0.0066C_{H_2O_2})$.

1. Introduction

Aluminum–water ($Al–H_2O$) mixtures offer promise for various applications, including space and underwater propulsion, hydrogen generation, and fuel cell technology ([1–3]). The combustion of nano-aluminum particles in water has been extensively studied in the recent past ([1,3–6]). The burning rates surpass those of many energetic materials, such as ammonium dinitramide (ADN) and hexanitrohexaazaisowurtzitane (CL-20) ([1,7]). At a pressure of 1 MPa, the burning rate of stoichiometric 38 nm $Al–H_2O$ mixture is 4.5 cm/s, which is nearly twice that of ADN [1]. For a particle size range of 38–130 nm, the burning rate is inversely proportional to particle size and has a pressure dependence of the form $r_b = ap^m$, with the exponent, m, in the range of 0.27–0.68, depending on the consistency of the mixture ([1,5]). The low burning-rate pressure exponents are beneficial for rocket motor performance, since they mitigate combustion instabilities and prevent motor failures [8]. For an equivalence ratio of 0.71, the specific impulse efficiency of 80 nm aluminum and ice (ALICE) mixture varies between 27 and 64%, depending on the motor size (1.91–7.62 cm) [4]. The measured specific impulse is in the range of 56–133 s, significantly lower than theoretical counterparts. This can be attributed to low combustion efficiencies (43–69%), caused by low reaction temperatures, insufficient residence times, and agglomeration of particles [4]. The high oxide (Al_2O_3) content in the particle also contributes the low adiabatic flame temperatures of ALICE mixtures. For example, the oxide layer constitutes ~25% of the particle mass when the particle size reaches 80 nm and the adiabatic flame temperature is ~2850 K at a pressure of 1 MPa [1]. The energy density can be enhanced by replacing a portion of nano-aluminum particles with micron-sized counterparts ([9]), since the active aluminum content of micron-sized particles is nearly 100%. The burning rates, however, decrease by a factor of four when the loading density of micron-sized particles reaches 80% [9]. New methods to promote the performance of aluminum–water mixtures are necessary.

Hydrogen peroxide (H_2O_2) has been used as monopropellant and oxidizer in liquid propellant rocket engines (LPREs) for various applications including rockets, jet-assisted take off (JATO) aircrafts, and attitude control system (ACS) engines [10]. Table 1 shows a

---

* Corresponding author. Fax: +1 404 894 2760.
E-mail address: vigor.yang@aerospace.gatech.edu (V. Yang).

http://dx.doi.org/10.1016/j.combustflame.2014.03.002
0010-2180/

Nomenclature

A	pre-exponential constant
C	concentration (weight percentage of hydrogen peroxide in oxidizer)
C_p	specific heat
D	diffusivity
d_p	particle diameter
E_A	activation energy
h_{fg}	enthalpy of vaporization
i	stoichiometric fuel-oxidizer mass ratio
k	velocity-to-thermal diffusivity ratio
k_B	Boltzmann constant
L	flame thickness
MW	molecular weight
n	entrainment index
N_A	Avogadro's number
O/F	oxidizer-to-fuel weight ratio
p	pressure
Q_r	heat of reaction
r_b	burning rate
R	gas constant
T	temperature
v	velocity
x	spatial coordinate
X_{eff}	effective oxidizer mole fraction
Y	mass fraction

Greek

ρ	density
δ_V	vapor zone thickness
α	thermal diffusivity
λ	thermal conductivity
τ_b	burning time
ϕ	volume fraction
σ	molecular diameter

Subscript

ad	adiabatic
b	burn
d	diffusion
f	flame, fluid
g	gas
ign	ignition
k	kinetic
l	liquid
m	mixture
O	oxidizer
p	particle
R	reaction zone
u	unburned
V	vapor zone
v	vaporization
L	liquid zone

comparison of the thermophysical properties of hydrogen peroxide and water. They have similar properties; the heat of formation of hydrogen peroxide (−187.80 kJ/mol), however, is greater than that of water (−285.80 kJ/mol). Hydrogen peroxide is thus considerably more energetic than water. One of the main drawbacks of hydrogen peroxide is self-decomposition during storage. It decomposes to form water vapor and oxygen gas

$$H_2O_2 \rightarrow H_2O + \frac{1}{2}O_2. \tag{1}$$

This process is enhanced by heat and catalyzed by impurities, water, and solid particles ([11,12]).

The addition of hydrogen peroxide to aluminum–water mixtures enhances the burning rates ([13,14]). Sabourin et al. [13] packed quasi-homogeneous mixtures of nano-aluminum particles, liquid water, and hydrogen peroxide in a quartz tube and measured the burning rates in an argon environment using an optical pressure vessel. The particle size was 38 nm and the active aluminum content 54.3%. The equivalence ratio was in the range of 0.50–1.25 and the concentration of hydrogen peroxide was varied between 0% and 35%. The concentration is defined as the weight percentage of hydrogen peroxide in oxidizer. For an equivalence ratio of 1.0 and pressure of 3.65 MPa, the burning rate increased by a factor of five, when the H_2O_2 concentration increased from 0 to 32%. Concentrations greater than 35% were not considered, due to an anomalous burning behavior characterized by over pressurization and rupture of the quartz tube. Zaseck et al. [14], similarly, measured the burning rates over a particle size range of 3–36 μm and H_2O_2 concentrations up to 90%. The oxidizer-to-fuel weight ratio was varied between 1.00 and 1.67. For a particle size of 19.86 μm and pressure of 6.9 MPa, the burning rate increased with increasing H_2O_2 concentration, from 0.43 cm/s at 30% to 1.38 cm/s at 90%.

Table 1
Thermophysical properties of hydrogen peroxide and water.

Property	Hydrogen peroxide	Water
Molecular weight (g/mol)	34.01	18.01
Density (g/cm^3)	1.45	1.00
Heat of formation* (kJ/mol)	−187.80	−285.80
Melting point (K)	272.72	273.15
Boiling point§ (K)	423.30	373.13
Heat of vaporization§ (kJ/kg)	1386	2260
Specific heat (kJ/kg-K)	2.36	4.18
Thermal conductivity (W/m-K)	0.46	0.58

[*] 298 K.
[§] 1 atm.

For aluminum–water mixtures, nano-particles must be used to achieve self-sustained flame propagation [1]. The situation becomes substantially different when hydrogen peroxide is used instead of water [14]. The advantages of micron-sized aluminum particles are the high active aluminum content and low cost. The active aluminum content of micron-sized particles is ~100%, which is nearly twice that of 38 nm particles (~54%). As a result, substantial enhancements in the flame temperature are obtained. For example, at a pressure of 3.65 MPa, the adiabatic flame temperature increases from 2500 to 3000 K, when the particle size increases from 38 nm to 1 μm. The cost of nano particles is at least an order of magnitude greater than micron counterparts [14]. It is worthwhile to mention that the reactivity of aluminum particles increases marginally when the particle size decreases below 20 μm [15]. The burning time of nano-aluminum particles is a weak function of particle size; it decreases by a factor of four, when the particle size decreases from 10 μm to 100 nm [15]. For these reasons, micron-sized particles are attractive for energy-conversion applications ([9,14]).

The obtained enhancements in the burning rate can be attributed to the high energy density of an Al–H_2O_2 system,

$$2Al + 1.5H_2O_2 \rightarrow Al_2O_3 + 1.5H_2, \tag{2}$$

$$2Al + 3H_2O \rightarrow Al_2O_3 + 3H_2. \tag{3}$$

The heat of Al–H_2O_2 reaction is −1388 kJ/mol, which is nearly twice that of Al–H_2O counterpart (−813 kJ/mol).

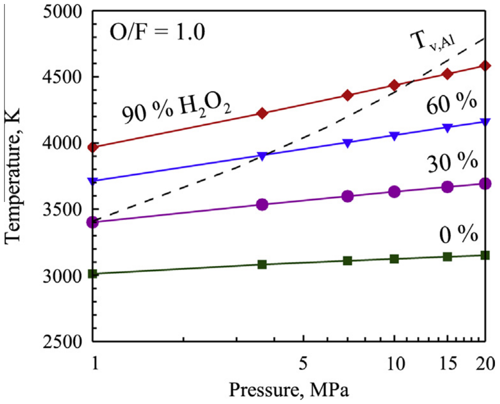

Fig. 1. Effect of pressure on aluminum vaporization temperature and adiabatic flame temperatures of aluminum, water, and hydrogen peroxide mixtures.

The mode of combustion can be altered by the addition of hydrogen peroxide. Figure 1 shows the effect of pressure on the adiabatic flame temperature of the aluminum–water–hydrogen peroxide system. The active aluminum content is 100% and the oxidizer-to-fuel (O/F) weight ratio is 1.0. The calculations were performed using NASA chemical equilibrium with applications (CEA) program [16]. At a pressure of 1 MPa, the flame temperature increases from 3011 to 3967 K, when the concentration of hydrogen peroxide increases from 0 to 90%. For H_2O_2 concentrations lower than 30%, the flame temperature is lower than the vaporization temperature of aluminum over a pressure range of 1–20 MPa. Heterogeneous reactions are thus expected to occur at the particle surface. For concentrations of 60% and 90%, homogeneous gas-phase reactions occur for pressures up to about 4 and 10 MPa, respectively. Figure 2 shows the effect of hydrogen peroxide on the sea-level specific impulse (I_{sp}) of aluminum–water mixture over a pressure range of 1–20 MPa. The active aluminum content is 100% and the exit pressure is 1 atm. The specific impulse increases by ~15 s when the concentration of hydrogen peroxide increases from 0 to 90%. Substitution of hydrogen peroxide for liquid water is thus beneficial for various propulsion and energy conversion applications.

In our previous work ([9,17,18]), a multi-zone theoretical framework was established to investigate the burning behaviors of nano-aluminum and water mixtures. The particle size was varied between 38 and 130 nm and the pressure range of interest was 1–10 MPa. Reasonably good agreement with experimental data was achieved. Key parameters that dictate the burning rate are found to be the thermal diffusivity of the mixture, heat of reaction, ignition temperature, particle burning time, and convective velocity of particles. The impact of entrainment and agglomeration of particles was also assessed. The particle size dependence of the burning rate stemmed from the particle burning time, whereas the pressure effect was attributed to the burning time and convective velocity of particles.

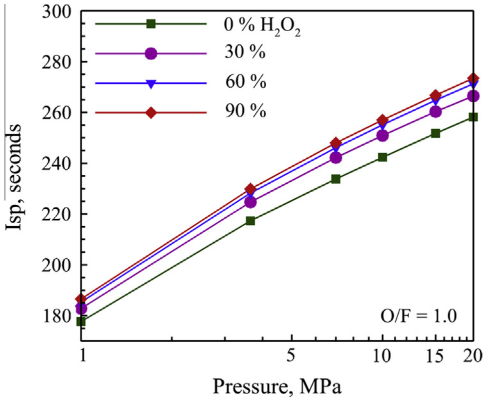

Fig. 2. Effect of pressure on specific impulse of aluminum–water–hydrogen peroxide mixtures for an exit pressure of 1 atm.

In the present study, the burning behaviors and combustion wave structures of aluminum-particle, water, and hydrogen-peroxide mixtures are explored. Emphasis is placed on the effects of pressure in the range of 1–20 MPa and particle size of 3–70 µm. Also considered are mixture ratio and concentration of hydrogen peroxide. Various controlling mechanisms and parameters are identified and studied systematically.

2. Theoretical framework

The present analysis treats one-dimensional, steady, planar, isobaric flame propagation in a quasi homogeneous mixture of aluminum particles, liquid water, and hydrogen peroxide. The particles are assumed to be uniformly sized and their agglomeration is neglected. A single temperature field is used to characterize the thermal behavior of the mixture. Figure 3 shows the physical model and multi-zone flame structure. The entire region of interest is divided into three different zones to demarcate the regions in which phase transition and chemical reaction occur. The liquid mixture of water and hydrogen peroxide undergoes thermodynamic phase transition at its vaporization front ($x = -\delta_v$). The particles begin to react at the ignition point ($x = 0$). Chemical reactions are neglected in the preheat zone. Mass and energy balances are enforced for a differential element in each zone. The resulting conservation equations are solved to obtain the burning rate and temperature distribution. The formulation is developed based on a coordinate system attached to the propagating flame.

2.1. Liquid zone (L)

The liquid zone extends from the vaporization front, $x = -\delta_v$, to the far field, $x = -\infty$. The energy conservation equation is given by

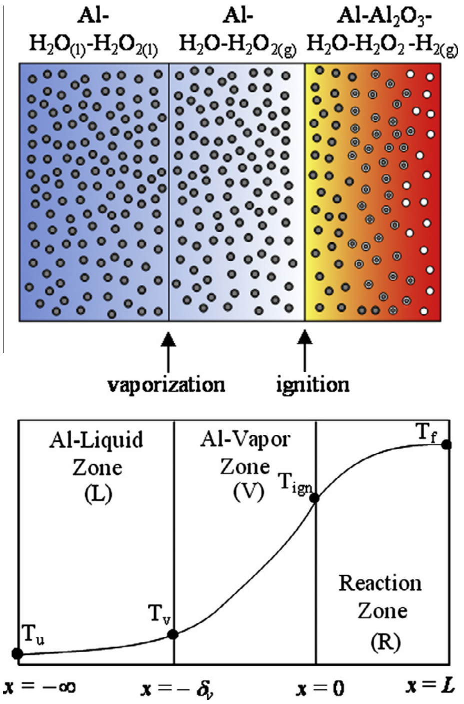

Fig. 3. Physical model and multi-zone flame structure (● Al, ○ Al_2O_3).

$$(\rho_{Al}C_{p,Al}\phi_{Al} + \rho_l C_{p,l}\phi_l) r_b \frac{dT}{dx} = \lambda_{m,L}\frac{d^2T}{dx^2}, \tag{4}$$

subject to the boundary conditions:

$$T_{x\to-\infty} = T_u; T_{x=-\delta_v} = T_v; \tag{5}$$

where ρ is the density, C_p the specific heat, r_b the burning rate, T the temperature, x the space coordinate, and δ_v the thickness of the vapor zone. The subscripts l, u, and v refer to the liquid, unburned state, and vaporization, respectively. An analytical expression for the temperature profile in the liquid zone is obtained as follows:

$$T = T_u + (T_v - T_u)\exp\{k_L(x + \delta_v)\}, \tag{6}$$

where $k_L = r_b/\alpha_{m,L}$ is the ratio of the burning rate to the thermal diffusivity of the mixture.

2.2. Vapor zone (V)

The oxidizer vaporizes at the vaporization front, $x = -\delta_v$, and rapidly flows through the interstitial space between particles. The gas velocity can be obtained by considering mass conservation at the interface

$$\rho_l r_b = \rho_g v_g. \tag{7}$$

Here, v is the velocity and the subscript g denotes gas. The energy equation can be expressed in the following form

$$(\rho_{Al}C_{p,Al}\phi_{Al} + \rho_l C_{p,g}\phi_l) r_b \frac{dT}{dx} = \lambda_{m,V}\frac{d^2T}{dx^2}, \tag{8}$$

subject to the interfacial conditions:

$$\begin{cases} x = -\delta_v : \lambda_m \frac{dT}{dx}\big|_V = \lambda_m \frac{dT}{dx}\big|_L + h_{fg}\phi_l\rho_l r_b, \\ x = 0 : T = T_{ign}, \end{cases} \tag{9}$$

where h_{fg} is the enthalpy of oxidizer vaporization and T_{ign} the ignition temperature of aluminum particles. The thickness of the vapor zone is obtained by enforcing heat-flux continuity at $x = -\delta_v$:

$$\delta_v = \frac{1}{k_V}\log\left\{\left(1 + \frac{\lambda_{m,V}k_V(T_{ign} - T_v)}{\lambda_{m,L}k_L(T_v - T_u) + h_{fg}\rho_l\phi_l r_b}\right)\right\}. \tag{10}$$

The temperatures at the interfacial boundaries are matched to provide a closed-form solution to the energy equation:

$$T = \frac{1}{1 - e^{-k_V\delta_v}}[T_v(1 - e^{k_V x}) - T_{ign}(e^{-k_V\delta_v} - e^{k_V x})]. \tag{11}$$

The temperature distribution in the preheat zone depends on the burning rate and thickness of the vapor zone, which are not known *a priori*.

2.3. Reaction zone (R)

Aluminum particles react with the gaseous oxidizer to form aluminum oxide and hydrogen gas (see Eqs. (2) and (3)). The energy equation can be written as

$$\sum_i \rho_i C_{p,i}\phi_i v_i \frac{dT}{dx} = \lambda_{m,R}\frac{d^2T}{dx^2} + \frac{\rho_m Q_r}{\tau_b}, \tag{12}$$

which is expressed as

$$\frac{d^2T}{dx^2} - \kappa\frac{dT}{dx} = -\frac{\rho_m Q_r}{\tau_b\lambda_{m,R}}, \tag{13}$$

subject to the boundary conditions:

$$\begin{cases} x = 0 : T = T_{ign}, \lambda_m \frac{dT}{dx}\big|_V = \lambda_m \frac{dT}{dx}\big|_R, \\ x = L : T = T_{ad}, \end{cases} \tag{14}$$

where $\kappa = \sum \rho_i C_{p,i}\phi_i v_i/\lambda_{m,R}$ is the ratio of the volume-averaged product of the density, specific heat, and velocity to the thermal conductivity of the mixture, Q_r the gravimetric heat of reaction, τ_b the particle burning time, and L the flame thickness. The subscripts *ad* and *i* refer to adiabatic and species *i*, respectively. The properties are calculated by averaging their respective values of the reactant and product species. The fluid velocity increases rapidly due to vaporization, and particles are transported by the gas flow, a phenomenon known as particle entrainment. Further details on the particle entrainment phenomenon and its effect on burning properties can be found in Ref. [18]. The particle velocity, v_p, can be expressed in the following form:

$$v_p = r_b\left(\frac{\rho_l}{\rho_g}\right)^n, \tag{15}$$

where n is the entrainment index, which varies between zero (no entrainment) and unity (complete entrainment). The flame thickness is thus given by

$$L = r_b\tau_b\left(\frac{\rho_l}{\rho_g}\right)^n. \tag{16}$$

The temperature profile in the reaction zone and heat-flux at the ignition point are obtained as follows:

$$T = \frac{\rho_m Q_r x}{\lambda_{m,R}\tau_b\kappa} + T_{ign}e^{\kappa x} + (1 - e^{\kappa x})\left(T_{ign} - \frac{1}{e^{\kappa L} - 1}\left[T_{ad} - T_{ign} - \frac{\rho_m Q_r L}{\lambda_{m,R}\tau_b\kappa}\right]\right). \tag{17}$$

$$\lambda\frac{dT}{dx}\bigg|_R = \frac{\rho_m Q_r}{\tau_b k} + \frac{\lambda k}{\exp(kL) - 1}\left[(T_f - T_{ign}) - \frac{\rho_m Q_r L}{\lambda\tau_b k}\right], \tag{18}$$

The product κL is significantly lower than unity, especially for pressures representative of those in practical applications [18]. For small values of κL, Eqs. (17) and (18) can be rewritten as

$$T = T_{ign} + \frac{x}{L}(T_{ad} - T_{ign}). \tag{19}$$

$$\lambda\frac{dT}{dx}\bigg|_R = \frac{\lambda}{r_b\tau_b}\left(\frac{\rho_g}{\rho_l}\right)^n(T_{ad} - T_{ign}). \tag{20}$$

The temperature varies linearly with spatial coordinate and the heat-flux is a constant in the reaction zone. Diwan et al. [19] packed magnesium–water mixtures in a quartz tube and measured the temperature profiles and burning rates at a pressure of 1 atm. The particle size was varied between 75 and 150 μm. In the reaction zone, a near-linear temperature profile was obtained, which justifies the assumption in the present work. The heat-flux at $x = 0$ in the preheat zone is given by

$$\lambda\frac{dT}{dx}\bigg|_V = r_b\left[2\frac{\rho_l\rho_p}{\rho_l + \rho_p}C_p(T_{ign} - T_u) + \frac{\rho_l\rho_p}{\rho_l + \rho_p}h_{fg}\right]. \tag{21}$$

By matching the two energy fluxes at the ignition point, the following expression for the burning rate is obtained:

$$r_b = \left[\frac{\lambda}{\rho_m C_p}\frac{2C_p(T_{ad} - T_{ign})}{2C_p(T_{ign} - T_u) + h_{fg}}\frac{1}{\tau_b}\frac{p^n}{R^n\overline{T}^n\rho_l^n}\right]^{1/2}, \tag{22}$$

where R is the gas constant and $\overline{T}$ the mean temperature in reaction zone. Eq. (22) resembles the Mallard-Le Chatelier formula [20] for the flame speed of a homogenous gas-phase mixture, except for the additional terms accounting for fluid vaporization and entrainment of particles. The burning rate is most sensitive to changes in the thermal diffusivity of the mixture, the flame temperature, and the ignition temperature, burning time, and entrainment index of particles. The entrainment index is treated as an adjustable parameter; its value is chosen in such a way that the model yields reasonably accurate predictions of the pressure exponent in the burning-rate law. For diffusion-controlled conditions, it can be deduced from Eq. (22) that the entrainment index is approximately twice the burning-rate pressure exponent.

2.4. Ignition temperature and burning time of aluminum particles

The present analysis requires as input parameters the ignition temperature and burning time of aluminum particles. Schoenitz et al. [21] investigated the oxidation of 3.0–4.5 μm aluminum particles in oxygen-argon-water vapor environment by thermogravimetric analysis at heating rates between 1 and 20 K/min. The oxidation behavior in water vapor was markedly different from that in oxygen; a stepwise weight change was observed at the melting point of aluminum (933 K) and the oxidation process was complete near 1273 K. Gurevich et al. [22], similarly, studied the ignition of micron-sized aluminum particles in a water vapor environment using torch and argon arc burners. The measured ignition temperatures in water vapor were significantly lower than the melting point of oxide film (2350 K), but were slightly greater than the melting point of aluminum (933 K). For example, the ignition temperatures of 5–25 μm particles were in the range of 1050–1300 K [22]. This phenomenon was attributed to the stabilization of porous γ-oxide polymorph [21] and/or formation of a weaker hydroxide layer on the particle surface [23]. For these reasons, the ignition temperature is taken as 933 K in the present study.

The burning time is yet another input parameter. Experimental data on burning time of aluminum particles in a hydrogen peroxide environment are not available. For diffusion-controlled conditions, the burning time is given by [24].

$$\tau_{b,d} = \frac{\rho_p d_p^2}{8\rho_g D \ln(1 + iY_{O,\infty})}, \tag{23}$$

where ρ is the density, D the diffusivity, d_p the particle diameter, i the stoichiometric fuel-oxidizer mass ratio, and Y the mass fraction. The subscripts p, g, and O refer to particle, gas, and oxidizer, respectively. The diffusivity of gases is given by [25].

$$D = \frac{2}{3}\left(\frac{k_B^3 T N_A}{\pi^3 MW}\right)^{1/2} \frac{T}{\sigma^2 p}, \tag{24}$$

where k_B the Boltzmann constant, MW the molecular weight, N_A Avogadro's number, p the pressure, and σ the molecular diameter. Substituting Eq. (24) into Eq. (23), the following expression for the burning time is obtained:

$$\tau_{b,d} = \frac{3\sigma^2 \pi^{3/2} \rho_p R_u d_p^2}{16 MW^{1/2} k_B^{3/2} N_A^{1/2} T^{1/2} \ln(1 + iY_{O,\infty})}. \tag{25}$$

The burning time is independent of pressure and inversely proportional to the square root of molecular weight of the gas. Beckstead [26] assimilated almost 400 data points for single-particle burning times in various oxidizer environments from more than ten different sources. The following particle burning-time correlation was established:

$$\tau_{b,d} = \frac{c_1 d_p^{1.8}}{T_0^{0.2} p^{0.1} X_{eff}}, \tag{26}$$

where X_{eff} is the effective oxidizer mole fraction, T_0 the initial temperature in Kelvin, d_p the particle diameter in μm, and c_1 a constant (=7.35×10^{-6}). The pressure exponent of 0.1 in Beckstead's correlation is not considered in the present study, for two reasons: (1) the diffusion time, in theory, is independent of pressure; (2) experimental data suggest that the burning time is independent of pressure above 20 atm [27]. The effective oxidizer concentration is written as

$$X_{eff} = X_{O_2} + 0.6X_{H_2O} + 0.22X_{CO_2}, \tag{27}$$

where X is the mole fraction. The burning time of aluminum particles in water is 66.67% greater than that in oxygen. This can be attributed to the fact that the burning time is inversely proportional to the square root of the molecular weight of the gas. Hydrogen peroxide decomposes to form water and oxygen, especially due to the catalytic effect of heat, water, and passivated aluminum particles (see Eq. (1)). The effective oxidizer mole fraction is thus given by

$$X_{eff} = 0.6X_{H_2O} + 0.73X_{H_2O_2}. \tag{28}$$

It can be deduced from Eq. (25) that the burning time of aluminum particles in hydrogen peroxide is lower than that in the decomposition product (H_2O/O_2 mixture) by ~20%. The burning rate of the mixture thus increases by ~10% when the decomposition process is not considered. The chemical kinetics of Al–H_2O_2 reaction are also poorly known. For kinetically-controlled conditions, the burning time is given by [15]

$$\tau_{b,k} = \frac{d_p^{0.3}}{pA\exp(-E_A/RT)X_{eff}}, \tag{29}$$

where E_A (=300 kJ/mol [14]) is the activation energy, p the gas pressure in atm, A the pre-exponential constant, and R the universal gas constant. Experimental data corroborate the fact that pressure and temperature of the gas exert a strong effect on the burning time in the kinetic regime [28]. The pre-exponential constant is treated as an empirical constant.

2.5. Thermophysical properties

Thermophysical properties are of paramount importance for predicting the burning behavior. The effective thermal conductivity of the mixture is calculated using the Maxwell–Eucken–Bruggeman (MEB) model ([29,30]), since it offers the most accurate predictions for all particle loading densities. Maxwell's theory assumes that the particles are dispersed from each other, while Bruggeman treats a random arrangement of fluid and particles [30]. The MEB model unifies the two theories by considering both dispersed and random distributions of the individual components. The resulting thermal conductivity of the mixture, λ_m, is given by ([29,30]).

$$\lambda_m = \frac{D + \sqrt{D^2 + 2\lambda_p\lambda_f}}{2},$$

$$D = (2\lambda_p - \lambda_f)\phi_p(1 - f_{p,d}) + (2\lambda_f - \lambda_p)\phi_f\left(\frac{2\phi_f + 2\phi_p f_{p,d} - 1}{2\phi_f}\right), \tag{30}$$

where λ is the thermal conductivity and ϕ the volume fraction. The subscripts m, p, and f refer to mixture, particle, and fluid, respectively. The thermal conductivity is determined iteratively, since the parameter $f_{p,d}$ is not known *a priori*. The procedure employed to calculate the unknown parameter can be found elsewhere ([29,30]). Figure 4 shows the thermal conductivity of the mixture as a function of particle volume fraction obtained using the MEB model. The entire domain can be divided into three regimes based on the particle volume fraction: (1) dilute regime, in which the thermal conductivity is nearly equal to that of the fluid ($\phi_p < 0.2$); (2) transition regime, in which significant deviations from fluid's thermal conductivity are first observed ($0.2 \leqslant \phi_p < 0.5$); (3) dense regime, in which the thermal conductivity increases sharply toward the maximum value ($\phi_p \geqslant 0.5$). The transition regime is of concern

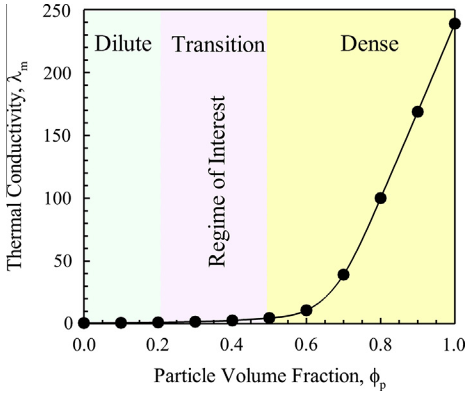

Fig. 4. Thermal conductivity of the mixture as a function of particle volume fraction; Maxwell–Eucken–Bruggeman model.

in the present study, since the volume fraction of particles varies in the range of 0.23–0.35. The thermophysical properties of aluminum and oxide are taken from Refs. [31–33], while those of water, hydrogen, and hydrogen peroxide are taken from Refs. [34–37]. Table 2 summarizes the property data at a baseline pressure of 3.65 MPa. All properties are evaluated at an average temperature in each zone. The fluid properties are weighted based on the concentration of hydrogen peroxide.

3. Results and discussion

The theoretical framework discussed in Section 2 is employed to calculate the flame structures and burning rates of aluminum particle, water, and hydrogen peroxide mixtures. Table 3 shows the characteristics of aluminum particles considered in the present study. To facilitate comparison with experimental data [14], particles with diameters in the range of 3–70 μm are considered. The active aluminum content of the particles is nearly 100%. The oxidizer-to-fuel weight ratio varies between 1.00 and 1.67 and the pressure range of interest is 1–20 MPa. Figure 5 shows the effect of pressure on the temperature distribution for a particle size of 20 μm and H_2O_2 concentration of 90%. The O/F ratio is unity. The flame thickness decreases from 0.28 to 0.14 mm, when the pressure increases from 1 to 20 MPa. A closed-form expression for the flame thickness, L, is given by

$$L = \left[\frac{\lambda}{\rho_m C_p} \frac{2C_p(T_{ad} - T_{ign})}{2C_p(T_{ign} - T_u) + h_{fg}} \tau_b \frac{\rho_l^n R^n \bar{T}^n}{p^n} \right]^{1/2}. \tag{31}$$

The thermophysical properties of the mixture are not strongly dependent on pressure. For diffusion-controlled conditions, pressure exerts a negligible effect on the burning time. The pressure dependence of flame thickness is thus mainly due to the entrainment phenomenon, since the particles move at lower velocities at higher pressures. It is apparent that the burning properties are dependent not only on the physicochemical properties of the mixture but also on the convective motion of the particles.

Table 3
Characteristics of aluminum particles [14].

Powder	Particle size (μm)	Al content (wt.%)
H-2	3	99.7
H-10	12	99.7
H-15	20	99.7
H-30	36	99.7
H-50	55	99.7
H-60	70	99.7

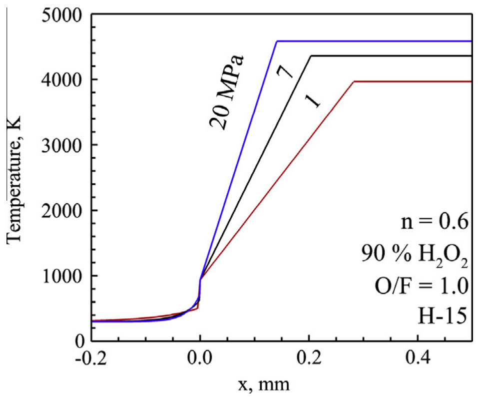

Fig. 5. Effect of pressure on the temperature distribution for a particle size of 20 μm and H_2O_2 concentration of 90%; O/F = 1.0.

Figure 6 shows the effect of H_2O_2 concentration on the temperature distribution for a particle size of 20 μm and pressure of 7 MPa. The O/F ratio is equal to 1.0. The flame thickness is weakly dependent on H_2O_2 concentration, increasing from 0.13 mm at 0% to 0.20 mm at 90%. The particle burning time is modestly affected by the substitution of hydrogen peroxide for liquid water. Hydrogen peroxide decomposes to form water vapor and oxygen gas; the oxidizing power of water vapor is 60% of that of oxygen. As a result, the burning time of 20 μm aluminum particles in hydrogen peroxide is 0.69 ms, which is lower than that in water (0.85 ms). The adiabatic flame temperature, however, is also a function of H_2O_2 concentration. At a pressure of 7 MPa, the flame temperature increases from 3110 to 4360 K, when H_2O_2 concentration increases from 0 to 100%. As a result, a thicker flame is obtained for a mixture with greater H_2O_2 concentration.

Figure 7 shows the effect of particle size on the temperature distribution for H_2O_2 concentration of 90% and pressure of 7 MPa. The O/F ratio is equal to 1.67. The burning time is a quadratic function of particle size, whereas the adiabatic flame temperature is independent of particle size. The flame thickness is thus greater for a larger particle.

Table 2
Thermophysical properties of different species in three zones at a baseline pressure of 3.65 MPa.*

Species	Thermal conductivity, W/m-K			Specific heat, kJ/kg-K			Density, kg/m^3		
	L	V	R	L	V	R	L	V	R
Aluminum	239	221	187	0.959	1.114	1.176		2700	
Aluminum oxide	–	–	5.406	–	–	1.344		4000	
Water	0.70	0.05	0.17	4.431	2.330	2.580	994	10.8	3.69
Hydrogen peroxide	0.50	0.05	0.14	2.618	1.727	2.386	1450	20.4	6.98
Hydrogen	–	–	1.08	–	–	17.124	–	–	0.41

L: liquid zone; V: vapor zone; R: reaction zone.
[*] T_{v,H_2O} = 519 K; h_{fg,H_2O} = 1737 kJ/kg; T_{v,H_2O_2} = 578 K; h_{fg,H_2O_2} = 1065 kJ/kg; T_{ign} = 933 K, T_{ad} = 3907 K at p = 3.65 MPa.

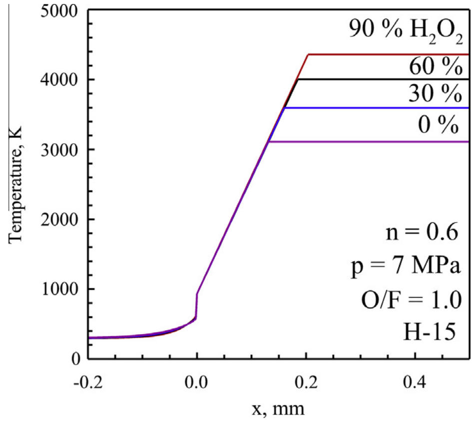

Fig. 6. Effect of H_2O_2 concentration on the temperature distribution for a particle size of 20 μm and pressure of 7 MPa; O/F = 1.0.

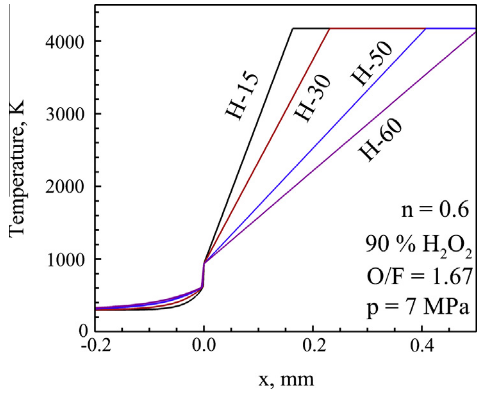

Fig. 7. Effect of particle size on the temperature distribution for H_2O_2 concentration of 90% and pressure of 7 MPa; O/F = 1.67.

The burning rate exhibits a pressure dependence of the form

$$r_b[\text{cm/s}] = a(p[\text{MPa}])^m, \tag{32}$$

where a is the pre-power factor and m the pressure exponent. Figure 8 shows the burning rate as a function of pressure for a particle size of 20 μm and H_2O_2 concentration of 90%. The O/F ratio varies in the range of 1.0–1.67. For the sake of consistency, the entrainment index is taken be equal to 0.6. The predicted burning-rate pressure exponent of 0.37 is slightly greater than the measured values (0.32–0.36). The pressure dependence of the burning rate stems from the fact that flame thickness decreases with increasing pressure, thereby enhancing the conductive heat flux at the ignition point. The burning rate is dependent on O/F ratio, decreasing from a value of 1.45 cm/s at O/F = 1.00 to 1.13 cm/s at O/F = 1.67. This can be attributed to the fact that the adiabatic flame temperature is maximum for stoichiometric conditions. For example, at a pressure of 7 MPa and H_2O_2 concentration of 90%, the flame temperature decreases from 4360 to 4176 K, when the O/F ratio increases from 1.00 to 1.67. The discrepancy between the predictions and experimental data varies in the range of 1–19%, depending on the pressure and O/F ratio. It is worth mentioning that the experimental measurements in the figure correspond to those obtained using the curve fit established by Zaseck et al. [14]. In reality, the burning rates were measured over a limited pressure range of 7–14 MPa. The discrepancy can be minimized by consideration of heat losses to the ambient environment. The impact of finite-rate kinetics on the burning rate may also be significant, especially at higher O/F ratios. Note that the burning rate is not extremely sensitive to changes in the flame temperature. This supports the hypothesis that combustion is controlled by the diffusion process rather than chemical kinetics. For kinetically-controlled conditions, temperature would exert a much stronger effect on the burning rate, since the reaction rate bears an exponential dependence on temperature.

Particle size exerts a strong effect on the burning rate in the size range of 20–70 μm. Figure 9 shows the effect of particle size on the burning rate for H_2O_2 concentration of 90% and O/F ratio of 1.67. The burning rate exhibits a particle size dependence of the form

$$r_b[\text{cm/s}] = c(d_p[\mu\text{m}])^{-0.85}, \tag{33}$$

where c is the pre-power factor. At a pressure of 7 MPa, the burning rate of 20 μm particles is 1.13 cm/s, which is significantly greater than that of the 70 μm counterpart (0.39 cm/s). A similar trend is observed for all pressures considered in the present study. The strong dependence of burning rate on particle size indicates the prevalence of diffusion-controlled combustion. The particle size, on the other hand, would exert a much weaker effect, should chemical kinetics be the rate-limiting process. In Ref. [15], $d_p^{-0.13}$ law is established for the flame speed under kinetically-controlled conditions. Note that the burning-rate pressure exponent is independent of particle size. The model slightly under-predicts the burning rates of H-30 particles. For example, at a pressure of 1 MPa, the predicted burning rate of 0.33 cm/s is lower than the experimental value of 0.4 cm/s. Particle size thus seems to exert a slightly weaker effect on the burning rate. The uncertainty in the measured size dependence of the burning rate is of concern, since only two sets of particle sizes in the diffusion regime were considered in experiments.

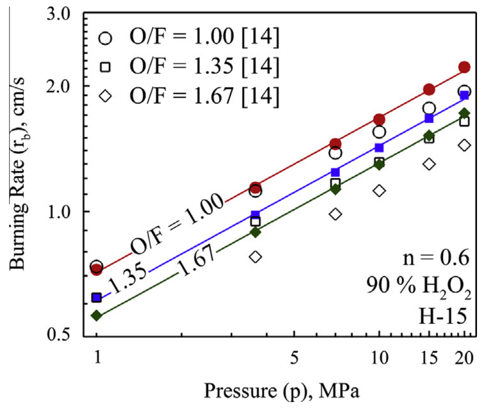

Fig. 8. Variation of burning rate with pressure for a particle size of 20 μm and H_2O_2 concentration of 90%. O/F = 1.00–1.67.

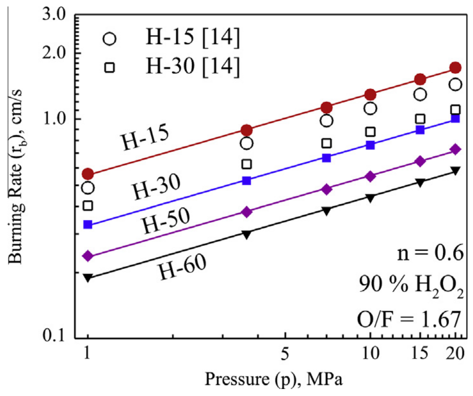

Fig. 9. Effect of particle size on the burning rate for H_2O_2 concentration of 90% and O/F ratio of 1.67.

The concentration of hydrogen peroxide in the oxidizer is yet another parameter that dictates the burning rate. Figure 10 shows the effect of H_2O_2 concentration on the burning rate for particle sizes of 20 and 36 μm and O/F ratio of unity. The burning rate is enhanced due to the substitution of hydrogen peroxide for water. At a pressure of 7 MPa and particle size of 36 μm, the burning rate increases from 0.48 to 0.86 cm/s, when H_2O_2 concentration increases from 0 to 90%. The model slightly over-predicts the burning rate of 20 μm particles for a concentration of 60%. For example, at a pressure of 10 MPa, the burning rate is predicted to be 1.36 cm/s, which is greater than the experimental value of 1.11 cm/s. This can be attributed to the importance of finite-rate kinetics and differences in the entrainment index, since the measured pressure exponent increases with decreasing H_2O_2 concentration [14]. The reaction temperature decreases from 4360 to 3110 K, when the H_2O_2 concentration decreases from 100 to 0%. As a result, both diffusion and kinetics may be rate-limiting for dilute concentrations. Better agreement with the experimental data is also obtained when the entrainment index is increased from 0.60 to 0.65. It is worthwhile to note that the obtained enhancement in the burning rate is primarily caused by changes in the adiabatic reaction temperature of the mixture. Greater enhancements are expected for smaller particles, which burn under temperature-sensitive kinetically controlled conditions.

As the particle size decreases below a cut-off value, the combustion mode begins to transition from diffusion to kinetically controlled conditions. Bazyn et al. [38] measured the cut-off particle size to be 10 μm at pressure of 8.5 MPa. Figure 11 shows the variation of burning rate with pressure for particle sizes of 3 and 20 μm and O/F ratio of unity. For 3 μm particles, the burning time is calculated using Eq. (29) and the pre-exponential constant is taken be equal to 2.18×10^8. The pressure exponent of 3 μm particles is 1.04, which is significantly greater than that of the 20 μm counterparts (0.37). The strong pressure dependence of the burning rate corroborates the fact the combustion of H-2 particles is controlled by chemical kinetics. Figure 12 shows the burning rate pressure exponent as a function of particle size for aluminum–water–hydrogen-peroxide mixtures. It increases from 0.35 to 1.04, when the particle size decreases from 70 to 3 μm. The results clearly show that the mode of combustion changes from diffusion to chemical kinetics when the particle size decreases below 20 μm.

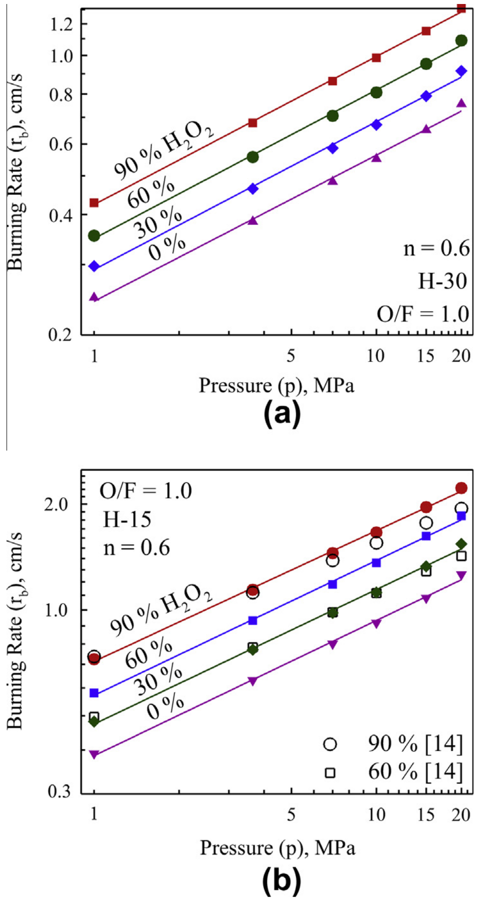

Fig. 10. Effect of H_2O_2 concentration on the burning rate for particle sizes of 20 and 36 μm and O/F ratio of 1.0.

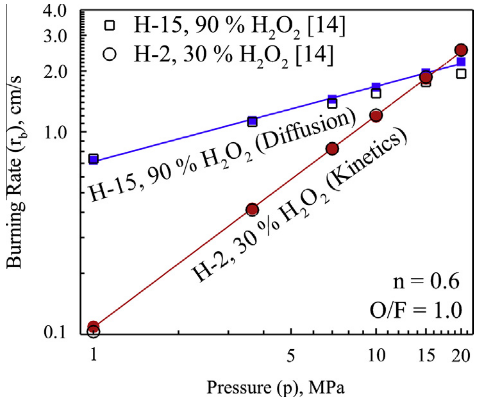

Fig. 11. Effect of pressure on the burning rate for particle sizes of 3 μm and 20 μm and O/F ratio of 1.0.

Figure 13 shows a comparison of the measured and calculated burning rates with those obtained using the following correlation

$$r_b[\text{cm/s}] = 4.97(p[\text{MPa}])^{0.37}(d_p[\mu\text{m}])^{-0.85}(\text{O/F})^{-0.54}\exp(0.0066C_{H_2O_2}), \tag{34}$$

where C_{H2O2} is the concentration of hydrogen peroxide. Reasonably good agreement is achieved, which demonstrates the validity of the correlation for the conditions encountered in the present study. Note that the correlation is valid only for particle sizes greater than 20 μm. For smaller particles, the effects of finite-rate kinetics may not be negligible and must be considered in the analysis.

A sensitivity analysis is conducted to determine the influences of uncertainties in various model parameters on the burning rate of the mixture. The ignition temperature of aluminum particles could be greater than the chosen value of 933 K, especially for larger particles. For example, Gurevich et al. [22] found that the

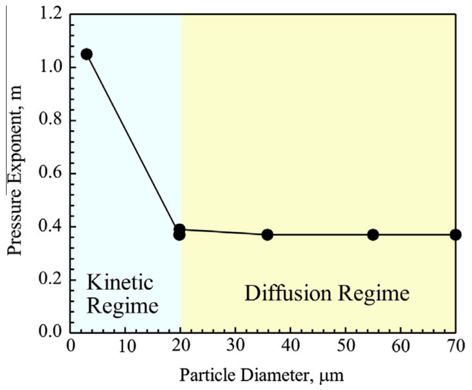

Fig. 12. Burning rate pressure exponent as a function of particle size for aluminum, water, and hydrogen peroxide mixtures.

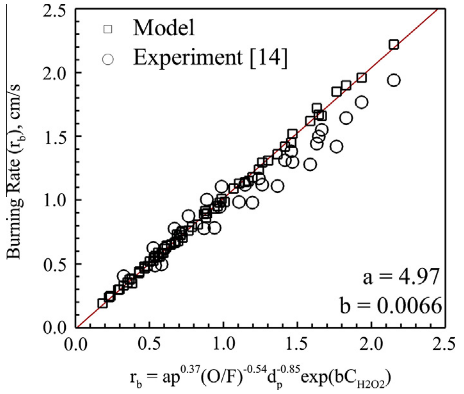

Fig. 13. Measured and calculated burning rates vs. curve-fit values for different pressures, particle sizes, O/F ratios, and H_2O_2 concentrations.

ignition temperatures of 5–25 μm aluminum particles in water were in the range of 1050–1300 K. The burning rate is modestly affected by changes in the ignition temperature. It decreases from 1.45 to 1.18 cm/s when the ignition temperature increases from 933 to 1300 K. Incomplete combustion of particles and heat losses to the ambient environment are two other phenomena of concern. The actual combustion temperature is lower than the theoretical counterpart when heat losses and incomplete combustion are considered. For example, the measured flame temperature of magnesium–water mixtures (75–150 μm) is 2050 K, significantly lower than the adiabatic value of 2750 K [19]. The burning rate decreases with decreasing flame temperature, from 1.45 cm/s at 4360 K to 1.23 cm/s at 3500 K. It is apparent that the effects of uncertainties in the ignition and combustion temperatures on the burning rate are comparable. For particles larger than 12 μm, the burning rate was assumed to be controlled by diffusion process. The effect of finite-rate kinetics could be significant especially at lower temperatures, since the burning time consists of contributions from both diffusion and chemical-kinetic processes. Note that the burning rate of the mixture decreases by ~30% when the particle burning time increases by a factor of two. A similar result is obtained when the thermal diffusivity of the mixture is halved. The entrainment index is another important parameter. In the present analysis, it is treated as an adjustable parameter to improve the model prediction of the burning-rate pressure exponent. A more complete multi-phase model taking into account momentum transfer with particles, particle–particle interactions, and wall effects is desired, so that the entrainment index can be treated as an eigenvalue of the analysis.

4. Conclusions

A theoretical analysis was performed to study the flame propagation of aluminum particle, liquid water, and hydrogen peroxide mixtures for particle sizes in the range of 3–70 μm and pressure of 1–20 MPa. The effect of hydrogen peroxide was studied systematically by replacing a portion of liquid water with hydrogen peroxide in the mixture in the amount of 0–90%. The entire region of interest was divided into preheat and reaction zones. The burning properties were determined by performing energy balance and enforcing the temperature and heat-flux continuities at the interfacial boundaries. The effective thermal conductivity of the mixture was calculated using the Maxwell–Eucken–Bruggeman model. Experimental data on ignition temperature and burning time of particles were incorporated into the analysis. Analytical expressions for the burning rate and flame thickness were obtained. The burning characteristics were dictated primarily by the thermal diffusivity of the mixture, flame temperature, ignition temperature, particle burning time, and entrainment index of particles. The burning rate correlated with pressure in the form of ap^m, where the exponent increased from 0.35 to 1.04, when particle size decreased from 70 to 3 μm. This trend was attributed to the transition of the combustion mode from diffusion to kinetically-controlled conditions. The burning rate was nearly doubled, when the concentration of hydrogen peroxide was increased from 0 to 90%. For particle sizes greater than 20 μm, a general correlation for the burning rate of the mixture was obtained, $r_b[\text{cm/s}] = 4.97 (p[\text{MPa}])^{0.37}(d_p[\mu\text{m}])^{-0.85}(\text{O/F})^{-0.54}\exp(0.0066C_{H_2O_2})$. For smaller particles, the effect of finite rate kinetics alters the influences of temperature, pressure, and particle size on the mixture burning rate. Future work must specifically examine the kinetics of Al–H_2O_2 reaction and determine its effect on the burning rate of sub-micron particles. Greater enhancements in the burning rate are expected with particles in this size range, since they burn under temperature-sensitive kinetically-controlled conditions.

Acknowledgments

The authors would like to thank the Air Force Office of Scientific Research (AFOSR) for their sponsorship of this program under Contract No. FA9550-13-1-0004. The support and encouragement provided by Dr. Mitat Birkan is greatly appreciated.

References

[1] G.A. Risha, J.L. Sabourin, V. Yang, R.A. Yetter, S.F. Son, B.C. Tappan, Combust. Sci. Technol. 180 (2008) 2127–2142.
[2] A. Ingenito, C. Bruno, J. Propul. Power 20 (2004) 1056–1063.
[3] E. Shafirovich, V. Diakov, A. Varma, Combust. Flame 144 (2006) 415–418.
[4] G.A. Risha, T.L. Connell Jr., R.A. Yetter, D.S. Sundaram, V. Yang, J. Propul. Power 30 (2014) 133–142.
[5] D.E. Kittell, L.J. Groven, T.R. Sippel, T.L. Pourpoint, S.F. Son, Combust. Sci. Technol. 185 (2013) 817–834.
[6] V.G. Ivanov, O.V. Gavrilyuk, O.V. Glazkov, M.N. Safronov, Combust. Expl. Shock Waves 36 (2000) 213–219.
[7] M.W. Beckstead, K. Puduppakkam, P. Thakre, V. Yang, Prog. Energy Combust. Sci. 33 (2007) 497–551.
[8] V. Yang, T.B. Brill, W.Z. Ren (Eds.), Solid Propellant Chemistry, Combustion, and Motor Interior Ballistics, AIAA Progress in Aeronautics and Astronautics, vol. 185, 2000.
[9] D.S. Sundaram, V. Yang, T.L. Connell Jr., G.A. Risha, R.A. Yetter, Proc. Combust. Inst. 34 (2013) 2221–2228.
[10] G.P. Sutton, History of Liquid Propellant Rocket Engines, American Institute of Aeronautics and Astronautics, Virginia, 2006.
[11] A. Hiroki, J.A. Laverne, J. Phys. Chem. B 109 (2005) 3364–3370.
[12] A.Z. Arutyunyan, G.L. Grigoryan, A.B. Nalbandyan, Kinet. Katal. 27 (1986) 1173–1178.
[13] J.L. Sabourin, G.A. Risha, R.A. Yetter, S.F. Son, B.C. Tappan, Combust. Flame 154 (2008) 587–600.
[14] C.R. Zaseck, S.F. Son, T.L. Pourpoint, Combust. Flame 160 (2013) 184–190.
[15] Y. Huang, G.A. Risha, V. Yang, R.A. Yetter, Combust. Flame 156 (2009) 5–13.
[16] B.J. Mcbride, S. Gordon, Computer Program for Calculation of Complex Chemical Equilibrium Compositions and Applications, Reference Publication 1311, NASA, 1996.
[17] D.S. Sundaram, V. Yang, Y. Huang, G.A. Risha, R.A. Yetter, Combust. Flame 160 (2013) 2251–2259.
[18] D.S. Sundaram, V. Yang, Combust. Flame 161 (2014) 2215–2217.
[19] M. Diwan, D. Hanna, E. Shafirovich, A. Varma, Chem. Eng. Sci. 65 (2010) 80–87.
[20] I. Glassman, R.A. Yetter, Combustion, fourth ed., Academic Press, 2008.
[21] M. Schoenitz, C.M. Chen, E.L. Dreizin, J. Phys. Chem. B 113 (2009) 5136–5140.
[22] M.A. Gurevich, K.I. Lapkina, E.S. Ozerov, Fiz. Goreniya Vzryva 6 (1970) 172–175.
[23] D.K. Kuehl, AIAA J. 3 (1965) 2239–2247.
[24] R.A. Yetter, G.A. Risha, S.F. Son, Proc. Combust. Inst. 32 (2009) 1819–1838.
[25] S.R. Turns, An Introduction to Combustion: Concepts and Applications, McGraw-Hill, second ed., 2006, p. 90.
[26] M.W. Beckstead, Combust. Expl. Shock Waves 41 (2005) 533–546.
[27] M. Marion, C. Chauveau, I. Gokalp, Combust. Sci. Technol. 116 (1996) 369–390.
[28] T. Bazyn, H. Krier, N. Glumac, Combust. Flame 145 (2006) 703–713.
[29] D.S. Sundaram, V. Yang, Effect of Packing Density on Flame Propagation of Nickel-Coated Aluminum Particles, Combust. Flame, 2014, Submitted for publication.
[30] J. Wang, J.K. Carson, M.F. North, D.J. Cleland, Int. J. Heat Mass Transfer 49 (2006) 3075–3083.

[31] W.F. Gale, T.C. Totemeier, Smithells Metals Reference Book, eighth ed., Elsevier, 2004.

[32] E.H. Buyco, F.E. Davis, J. Chem. Eng. Data 15 (1970) 518–523.

[33] R.G. Munro, J. Am. Ceram. Soc. 80 (1997) 1919–1928.

[34] E.W. Lemmon, M.L. Huber, M.O. McLinden, Reference Fluid Properties, National Institute of Standards and Technology, 2007.

[35] J.V. Sengers, J.T.R. Watson, J. Phys. Chem. Ref. Data 15 (1986) 1291–1314.

[36] R.J. Kee, M.E. Coltrin, P. Glarborg, Chemically Reacting Flow: Theory and Practice, John Wiley & Sons, New Jersey, 2003.

[37] R.A. Svehla, Estimated Viscosities and Thermal Conductivities of Gases at High Temperatures, NASA Technical, Report R-132, 1962.

[38] T. Bazyn, H. Krier, N. Glumac, Proc. Combust. Inst. 31 (2) (2007) 2021–2028.